Tự động nhận dạng và đánh giá mức độ nghiêm trọng của khối u não bằng các phương pháp học sâu

TÓM TẮT

Nghiên cứu này đề xuất một phương pháp tự động để phát hiện và đánh giá mức độ nghiêm trọng của khối u não từ ảnh cộng hưởng từ (MRI) bằng cách sử dụng mô hình học sâu ResU-Net. Dữ liệu MRI, được lấy từ bộ dữ liệu LGG Segmentation trên Kaggle, bao gồm hình ảnh của các bệnh nhân được chẩn đoán mắc khối u não. Sau bước tiền xử lý, dữ liệu được chia thành các tập huấn luyện, xác thực và kiểm thử. Mô hình ResU-Net được huấn luyện để phân đoạn và phát hiện sự hiện diện của khối u não. Ngoài ra, diện tích vùng khối u cũng được tính toán nhằm hỗ trợ đánh giá mức độ nghiêm trọng của bệnh. Hiệu suất của ResU-Net được so sánh với các kiến trúc học sâu khác, bao gồm U-Net, FC-DenseNet và DeepLabv3+. Kết quả thực nghiệm cho thấy ResU-Net đạt độ chính xác phát hiện cao nhất (94%) và Điểm Dice ấn tượng (92%), cùng với sai số ước lượng diện tích khối u thấp nhất trong số các mô hình được đánh giá. Những phát hiện này nhấn mạnh tiềm năng mạnh mẽ của ResU-Net trong việc hỗ trợ hiệu quả quá trình chẩn đoán và lập kế hoạch điều trị cho các trường hợp u não.

Từ khóa: *Phát hiện khối u tự động, Khối u não, Học sâu, Ảnh cộng hưởng từ (MRI), ResU-Net.*

Automatic Detection and Severity Assessment of Brain Tumors Using Deep Learning Approaches

ABSTRACT

This study proposes an automated method for detecting and assessing the severity of brain tumors from magnetic resonance imaging (MRI) using a deep learning model, ResU-Net. The MRI data, sourced from the LGG Segmentation dataset on Kaggle, consist of images from patients diagnosed with brain tumors. After pre-processing, the data were split into training, validation, and testing sets. The ResU-Net model was trained to segment and detect the presence of brain tumors. Additionally, the tumor region area was calculated to support the evaluation of disease severity. The performance of ResU-Net was compared with other deep learning architectures, including U-Net, FC-DenseNet, and DeepLabv3+. Experimental results show that ResU-Net achieved the highest detection accuracy (94%) and an impressive Dice Score (92%), along with the lowest tumor area estimation error among the models evaluated. These findings highlight the strong potential of ResU-Net in effectively supporting the diagnosis and treatment planning of brain tumor cases.

Keywords: *Automatic tumor detection, Brain tumor, Deep learning, Magnetic Resonance Imaging (MRI), ResU-Net.*

1. INTRODUCTION

Brain tumors result from the abnormal and uncontrolled growth of cells within the brain.[1-3] They are generally classified into two categories: benign and malignant. Both types can pose serious health risks, with malignant tumors typically exhibiting rapid growth and the potential to invade or metastasize to other parts of the body. Brain tumors are commonly diagnosed through imaging techniques such as CT, MRI, and PET, or via clinical tests including biopsy and cerebrospinal fluid analysis.[4-6] Early detection plays a critical role in improving treatment outcomes and increasing the survival rate of patients.

In recent years, artificial intelligence (AI), particularly deep learning techniques, has experienced rapid advancements and opened up a wide range of applications across various domains, especially in healthcare.[7,8] In the field of medical imaging, deep learning architectures such as GoogLeNet, U-Net, VGG, ResNet, Inception, DenseNet, and DeepLab have been widely adopted for brain tumor detection and classification tasks.[9-12] One of the most prominent applications is the identification and classification of brain tumors from magnetic resonance imaging (MRI), which greatly assists physicians in making accurate diagnoses and formulating effective treatment plans.[13,14] The integration of deep learning into medical practice promises higher diagnostic accuracy, reduced processing time, and minimized subjectivity compared to traditional diagnostic approaches.

Among deep learning models, the U-Net is one of the most pioneering and widely adopted architectures for brain tumor segmentation in medical imaging.[15] Variants of U-Net, such as ResU-Net[16], FC-DenseNet[17], and DeepLabv3+[18], have been developed to further enhance feature extraction capabilities and improve segmentation accuracy. However, the performance of each model varies depending on the dataset characteristics and training conditions.

U-Net follows a symmetric encoder–decoder architecture, connected through a central bottleneck. The encoder is responsible for extracting hierarchical features via convolutional blocks (ConvBlock) and progressively reducing spatial resolution using max pooling layers [19]. Conversely, the decoder restores the original image resolution through upsampling layers (UpConv), while incorporating corresponding features from the encoder via skip connections. These skip connections help retain important

spatial details that may be lost during downsampling. Typically, the input MRI image has a size of 256×256×3, and the output is a binary segmentation map of size 256×256×1[20], representing the tumor region.

ResU-Net is constructed based on a symmetric encoder–decoder architecture similar to U-Net, with the key distinction being the replacement of standard convolutional blocks by ResNet blocks.[21] The integration of internal residual connections enhances feature extraction capability and mitigates information loss during. The image resolution is progressively downsampled from 256×256 → 128×128 → 64×64 → 32×32 → 16×16, while the number of feature maps increases accordingly to capture deeper semantic representations.

On the other hand, FC-DenseNet leverages Dense Blocks to promote feature reuse.[22,23] Its architecture also comprises three main components: encoder, bottleneck, and decoder. The encoder processes the input image of size 256×256×3 using a 3×3 convolution layer with 48 filters to extract initial features. This is followed by multiple Dense Blocks, each consisting of densely connected convolutional layers, which significantly enhance feature learning. Between these blocks, Transition Down layers (composed of convolution and pooling) is applied to reduce spatial resolution. The bottleneck section utilizes a specialized Dense Block with a higher number of filters to optimize deep feature learning before transitioning to the decoder.[24,25] The decoder includes Transition Up layers (via upsampling or transposed convolution) to restore the image resolution, followed by Dense Blocks to recover detailed information. Skip connections from the encoder are incorporated to retain essential spatial features. The final output is a binary segmentation map of size 256×256×1, accurately highlighting the tumor region in the brain image.

DeepLabV3+ adopts an encoder–decoder architecture but introduces several notable enhancements compared to previous models.[16,26] (1) The input image of size 256×256×3 is passed through a pre-trained Xception feature extractor, a deep neural network known for its strong feature extraction capability. The model incorporates two skip connections from intermediate layers (16×16×1024 and 32×32×256) to retain multi-scale spatial information. (2) A key component of this architecture is the Atrous Spatial Pyramid Pooling (ASPP) module, which captures global contextual information at multiple scales using atrous (dilated) convolutions. This design improves the model's ability to detect objects of varying sizes and shapes, such as brain tumors. (3) After merging the features from ASPP and the skip connections, the model applies further convolutional layers and a final upsampling step to produce a binary output image of size 256×256×1 representing the segmented tumor region.

This study proposes a deep learning-based approach using the ResU-Net model for brain tumor classification and severity assessment based on tumor area. MRI brain images from the publicly available LGG Segmentation dataset were preprocessed through contrast enhancement, normalization to the range [0, 1], and binary labeling (tumor vs. non-tumor). The processed data were split into training, validation, and test sets for training the ResU-Net model. Tumor area was computed as an indicator of disease severity. To evaluate the effectiveness of the proposed method, ResU-Net was compared with other deep learning models using the same dataset. Experimental results demonstrate that ResU-Net outperformed other models in both classification accuracy and tumor area estimation. These findings underscore the potential of ResU-Net for real-time automatic brain tumor detection and severity evaluation in clinical applications.

2. RESEARCH METHODOLOGY

The dataset used in this study is the LGG Segmentation Dataset (Low-Grade Glioma). It contains 3D MRI images of patients diagnosed with low-grade brain tumors. The data origin is detailed in the study conducted by the Cancer Genome Atlas Research Network. Both tumor and non-tumor images were split into training, testing, and validation sets in a (70:10:20) ratio, as illustrated in Figure 1. The entire workflow of the proposed method consists of data preprocessing, model construction, training, performance evaluation, and comparison.

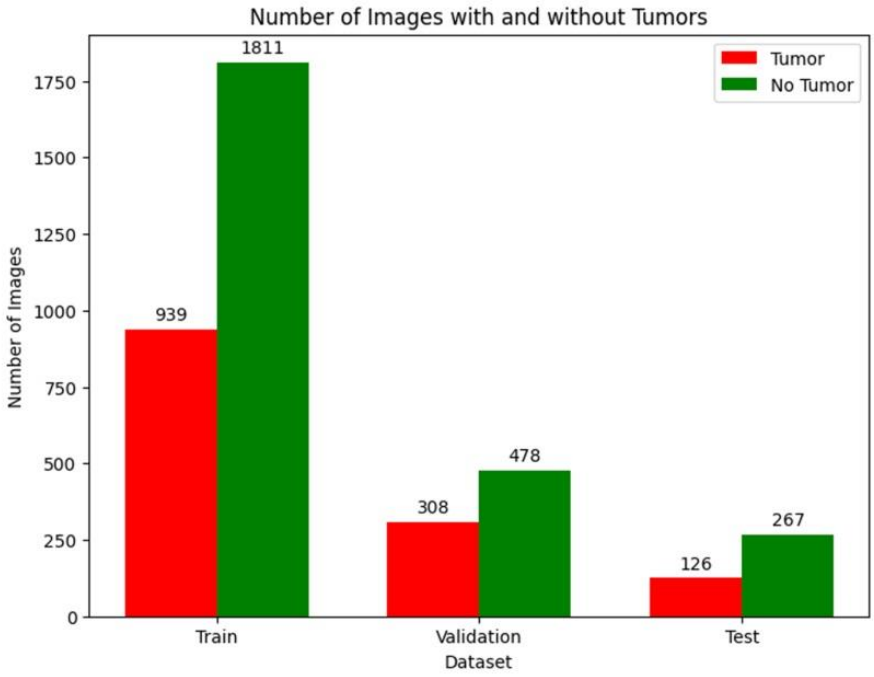

Figure 1. The dataset is split into (Train:Test:Validation) in a (70:10:20) ratio.

In this study, Google Colab is utilized as the programming environment, integrated with GPU hardware to optimize the training process of deep learning models. The hardware setup includes an NVIDIA A100-SXM4-40GB GPU with 42.5 GB of VRAM, an Intel(R) Xeon(R) CPU running at 2.20GHz, 89.6 GB of RAM, and 50 GB of storage via Google Drive. The main programming language used is Python 3.10. The software stack includes TensorFlow 2.11, Keras, and PyTorch for deep learning, along with NumPy, Pandas, OpenCV, Matplotlib, and Seaborn for data processing and visualization.

2.1. Data pre-processing

Figure 2 illustrates an example of an original MRI scan (Figure 2(a)) and its corresponding mask (Figure 2(b)) from the LGG Segmentation Dataset. The 3D MRI volumes in the dataset are sliced into 2D images and resized to a standardized resolution of 256×256 pixels. The preprocessing steps include intensity normalization to balance the image contrast, scaling pixel values to the [0, 1] range, and converting labels into binary format to distinguish between tumor and non-tumor brain images.

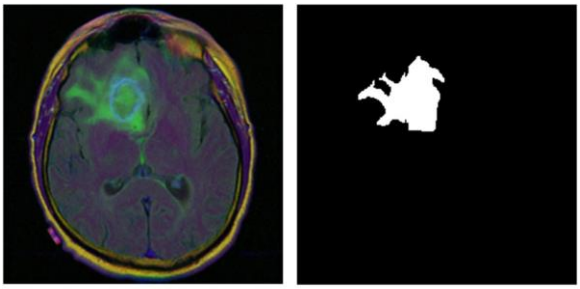

Figure 2. Original MRI image (a) and its corresponding mask (b) from the LGG segmentation dataset.

In this study, the ResU-Net model is employed for brain tumor segmentation and tumor area estimation. Its performance is compared against three other models: U-Net, FC-DenseNet, and DeepLabV3+. All models are trained under the same conditions, including 200 training epochs, an initial learning rate of 0.001, the Adam optimizer, and the Dice Loss function as the evaluation metric.

2.2. ResU-Net deep learning architecture

ResU-Net is an enhanced variant of the U-Net architecture that incorporates residual blocks to improve gradient flow during deep network training. Figure 3 illustrates the overall structure of the ResU-Net model. Similar to U-Net, ResU-Net consists of two main components: an encoder and a decoder. In the encoder block, ResNetConv modules are employed to enhance feature extraction capabilities and mitigate

information loss during backpropagation, thanks to internal residual connections [10, 11]. The spatial resolution of the feature maps is progressively reduced through the layers: from 256×256 → 128×128 → 64×64 → 32×32 → 16×16, while the number of feature channels increases.

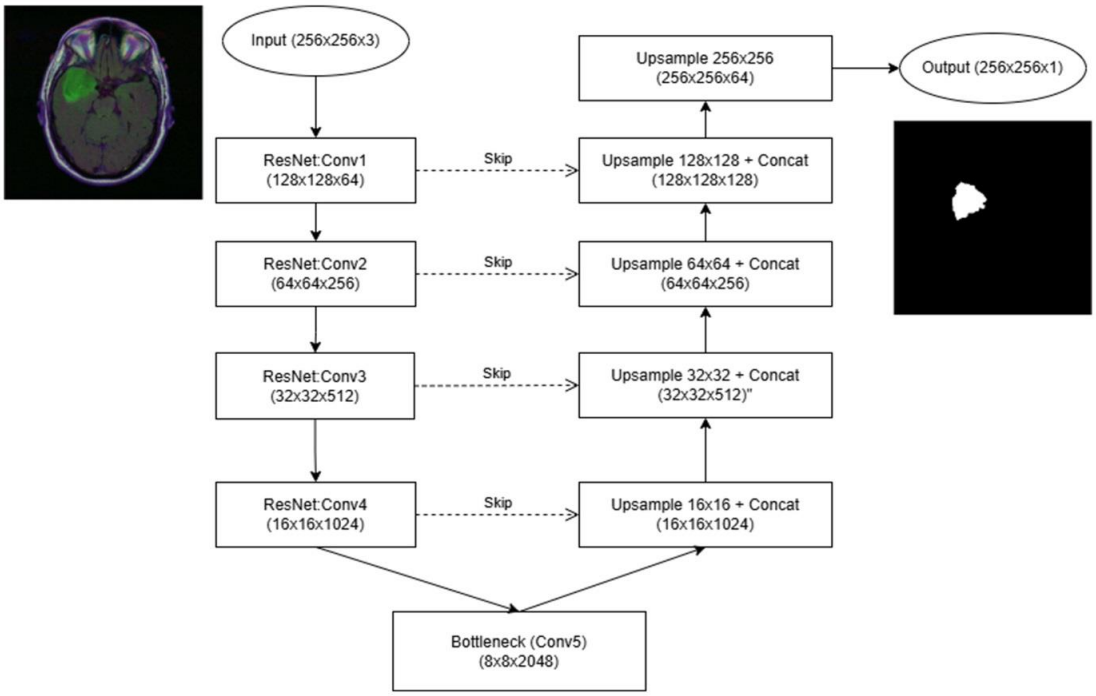

Figure 3. Architecture of the ResU-Net model[31]

The decoder block utilizes up-sampling layers to restore the original image resolution and integrates contextual information from the encoder via skip connections, which help to accurately recover fine image details. The final output of the ResU-Net model is a binary image of size 256×256×1, representing the segmented brain tumor region.

2.3. Model evaluation metrics

To evaluate the performance of the segmentation models, this study employs commonly used metrics, including Accuracy, Precision, Recall, F1-Score, IoU, and Dice Coefficient.[27,28] The formulas for these metrics are presented as follows:

Accuracy: The ratio of correctly classified pixels (both tumor and non-tumor regions) to the total number of pixels. However, accuracy can be misleading in the case of imbalanced data (e.g., the tumor region is much smaller than the background).

Precision (Positive Predictive Value): Indicates how many of the pixels predicted as tumor by the model is actually tumor pixels. High precision means the model generates fewer false positives.

Recall (Sensitivity): The proportion of actual tumor pixels correctly identified by the model. High recall ensures that tumor regions are not missed.

F1-Score: The harmonic mean of Precision and Recall, providing a balanced assessment between false positives and false negatives.

IoU (Intersection over Union): Measures the overlap between the predicted segmentation and the ground truth, calculated as the ratio of their intersection over their union. It is widely used in segmentation tasks.

Dice Coefficient: Similar to IoU but places more emphasis on the overlapping region. It is frequently used in medical image analysis due to its ability to accurately evaluate small lesion regions.

All these metrics are calculated on the test set and are used to objectively compare the performance of different models.

2.4. Tumor severity assessment

To evaluate the severity of a brain tumor, one of the key metrics is its area. By comparing the tumor area in the current MRI scan with previous scans, specialists can assess the effectiveness of the treatment. For instance, if the tumor area remains unchanged, it suggests

that the treatment is effectively halting tumor growth. Conversely, an increase in tumor size indicates disease progression and implies that the current treatment regimen may be ineffective and needs revision.

In this study, two methods are proposed for calculating the tumor area. One of them involves calculating the area based on the number of pixels identified as tumor regions in the MRI image. To compute the tumor area, the resolution of the MRI image in DPI (Dots Per Inch) is considered. The total tumor area is then given by

$$S_T = N_p \times S_p \quad (1)$$

Where, S_T is the tumor area (mm²), N_p is the number of pixels identified as tumor tissue by the deep learning model. For MRI images with a DPI of 96, the side length of one pixel is calculated as $1\text{pixel} = \frac{25.4\text{mm}}{96} \approx 0.265\text{mm}$. Thus, the area of a single pixel is $S_p = 0.265^2 \approx 0.07\text{mm}^2$.

3. RESULTS AND DISCUSSION

3.1 Training performance evaluation

During the training phase, two key metrics were used to preliminarily assess the performance of the models: Dice Coefficient and Loss. Figure 4 and 5 illustrate the evolution of the Dice Coefficient and Loss values, respectively, throughout the training and validation processes for the four segmentation models: U-Net, ResU-Net, FC-DenseNet, and DeepLabV3+.

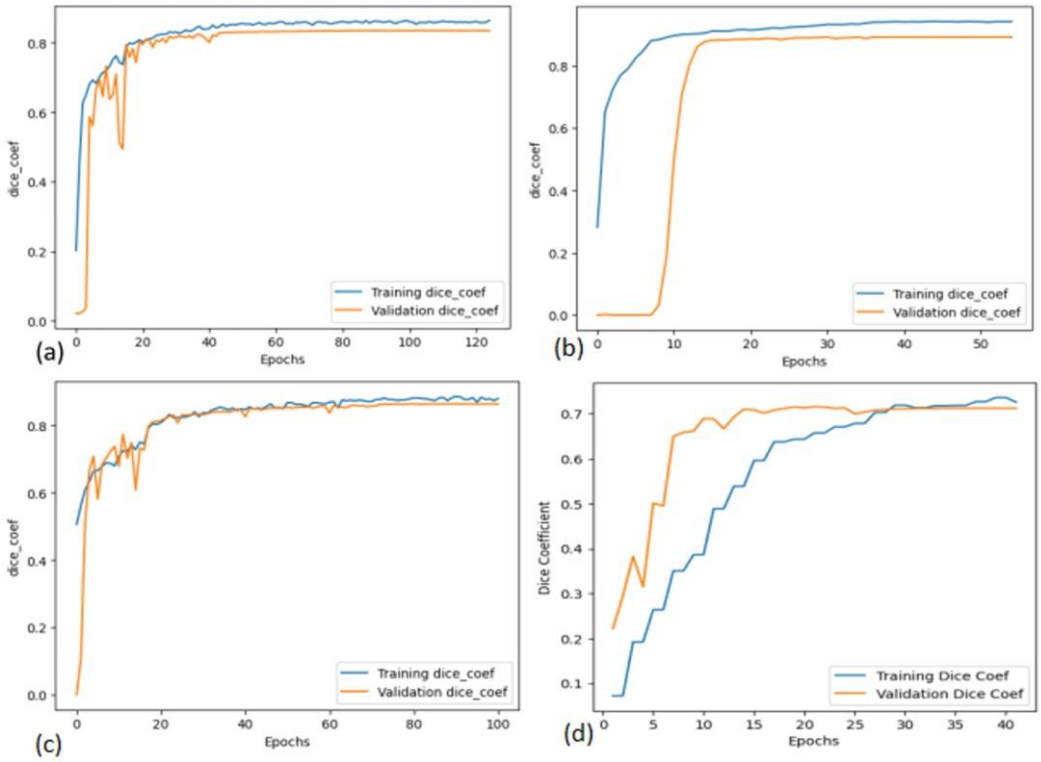

Figure 4. Dice Coefficient plots for (a) U-Net, (b) ResU-Net, (c) FC-DenseNet, and (d) DeepLabV3+.

In terms of the Dice Coefficient, U-Net and FC-DenseNet achieved faster convergence (within 10 epochs) compared to ResU-Net and DeepLabV3+. Although ResU-Net required a longer convergence time, it achieved the highest segmentation accuracy of approximately 90% (see Figure 4b), while U-Net and FC-DenseNet both reached around 85% accuracy (Figure 4a and 4c). Among all models, DeepLabV3+ demonstrated the weakest performance, with slower convergence (around 25 epochs) and the lowest accuracy (approximately 70%) as shown in Figure 4d. Regarding the Loss metric, ResU-Net again showed superior performance, with the loss value approaching zero (Figure 5b). In contrast, the other three models maintained higher loss values around 0.2 (Figure 5a, 5c, and 5d).

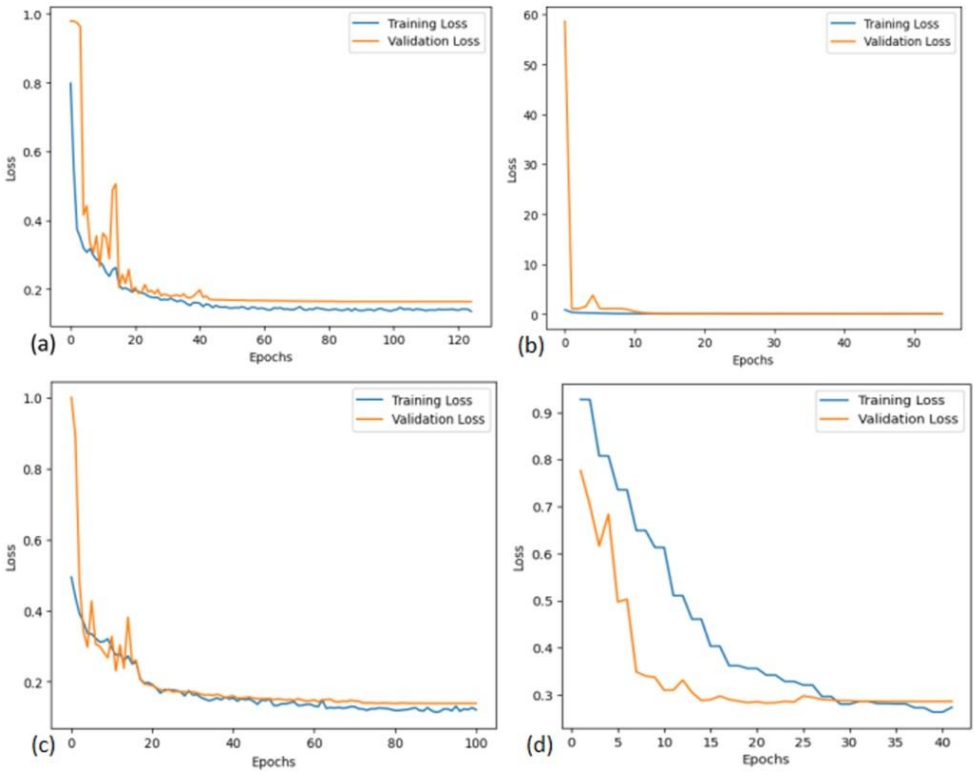

Figure 5. Loss plots for (a) U-Net, (b) ResU-Net, (c) FC-DenseNet, and (d) DeepLabV3+.

Table 1 presents a comparative analysis of Dice Coefficient and Intersection over Union (IoU) metrics for four deep learning models: U-Net, ResU-Net, FC-DenseNet, and DeepLabV3+, across training, validation, and testing datasets. Among these models, ResU-Net demonstrates superior performance across all three data splits. It achieves the highest Dice scores of 96% (Train), 90% (Validation), and 92% (Test), and corresponding IoU scores of 94%, 87%, and 90%, respectively. These results indicate that ResU-Net not only learns effectively from the training data but also generalizes well to unseen data.

Table 1. Dice Coefficient and IoU Scores of Different Models on Train, Validation, and Test Sets.

Model	DICE-COEF			IoU		
	Train	Val	Test	Train	Val	Test
U-Net	0.89	0.85	0.85	0.86	0.82	0.82
ResU-Net	0.96	0.90	0.92	0.94	0.87	0.90
FC-DenseNet	0.92	0.87	0.89	0.89	0.83	0.87
DeepLabV3+	0.89	0.85	0.88	0.84	0.80	0.85

FC-DenseNet also performs competitively, achieving Dice scores of 92%, 87%, and 89%, and IoU scores of 89%, 83%, and 87% for the same respective datasets. While slightly lower than ResU-Net, FC-DenseNet outperforms both U-Net and DeepLabV3+. Despite being a state-of-the-art segmentation model, DeepLabV3+ shows relatively moderate performance, with Dice scores of 89%, 85%, and 88%, and IoU scores of 84%, 80%, and 85%. These are comparable to or slightly better than U-Net, which scores 85%–89% (Dice) and 82%–86% (IoU), but fall short of the results achieved by ResU-Net and FC-DenseNet. In summary, ResU-Net achieves the best balance between learning capacity and generalization, making it the most effective model for brain tumor segmentation in this study.

3.2 Brain tumor classification performance evaluation

Figure 6 illustrates the confusion matrices for

four models (U-Net, ResU-Net, FC-DenseNet, and DeepLabv3+) in classifying brain MRI images into two categories: "Tumor" and "No Tumor." Each matrix presents the number of correctly and incorrectly classified MRI images.

The U-Net model correctly classified 247 non-tumor images and 110 tumor images, but misclassified 20 non-tumor images as tumors and 16 tumor images as non-tumor (see Figure 6(a)).

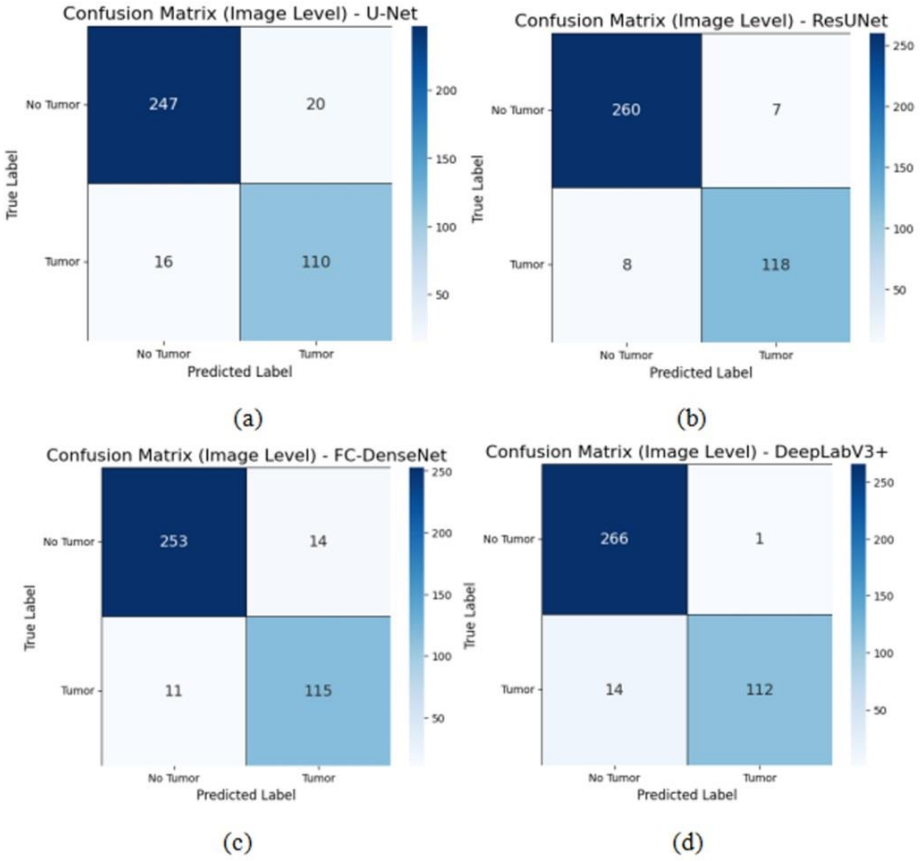

Figure 6. Confusion matrices of the models: (a) U-Net model; (b) resU-Net model; (c) FC-DenseNet model; (d) DeepLabv3+ model.

The ResU-Net model achieved better performance, correctly identifying 260 non-tumor and 118 tumor images, with only 7 non-tumor and 8 tumor images misclassified (see Figure 6(b)). FC-DenseNet correctly classified 253 non-tumor and 115 tumor images, while misclassifying 14 non-tumor and 11 tumor images (see Fig. 6(c)).

DeepLabv3+ yielded the highest overall accuracy, with 266 non-tumor and 112 tumor images correctly identified. However, it still misclassified 1 non-tumor and 14 tumor images (see Figure 6(d)). Generally, ResU-Net demonstrated a balanced performance across both classes, whereas DeepLabv3+ excelled in detecting non-tumor images but was slightly less accurate in identifying tumor cases. These results suggest that selecting the appropriate model depends on the dataset characteristics and application priorities whether maximizing tumor detection or minimizing false alarms.

3.3 Segmentation and prediction results evaluation

Figure 7 shows the prediction results for two brain MRI images without tumors (Fig. 7(a)), using four deep learning models: U-Net (Figure 7(c)), ResU-Net (Figure 7(d)), FC-DenseNet (Figure 7(e)), and DeepLabV3+ (Figure 7(f)). The experimental results indicate that all four models achieved 100% accuracy in correctly identifying tumor-free MRI scans.

Figure 8 showcases the segmentation results of brain tumors from three different MRI scans using four deep learning models. For each case, the figure displays the original MRI image, the ground truth mask, and the predicted masks from U-Net, ResU-Net, FC-DenseNet, and DeepLabV3+. The findings reveal that while all models can detect tumor regions, their accuracy and consistency vary: (1) ResU-Net and FC-DenseNet exhibit the closest agreement with the ground truth, particularly for tumors with regular, simple shapes; (2) U-Net sometimes produces incomplete or irregular segmentations, especially along tumor boundaries; and (3) DeepLabV3+ delivers well-defined boundaries for large tumors but tends to blur or

overestimate boundaries in cases of small or irregularly shaped tumors.

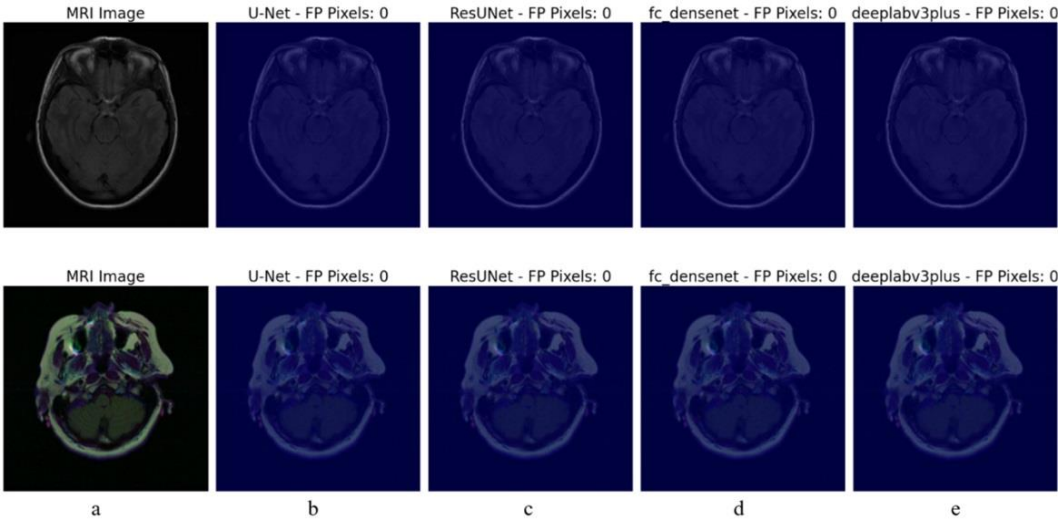

Figure 7. MRI images without brain tumors: (a) original MRI images; (b) ground truth masks; (c) predicted masks by U-Net; (d) by ResU-Net; (e) by FC-DenseNet; (f) by DeepLabV3+.

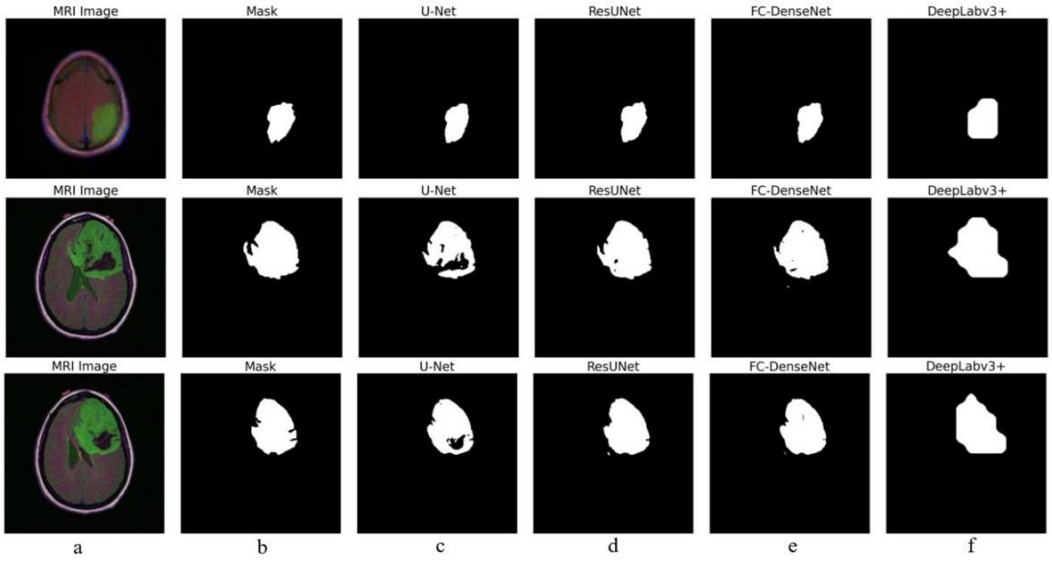

Figure 8. MRI images with brain tumors: (a) original MRI images; (b) ground truth masks; (c) predicted masks by U-Net; (d) by ResU-Net; (e) by FC-DenseNet; (f) by DeepLabV3+.

Figure 9 presents tumor segmentation results on two MRI images, along with key quantitative metrics including Tumor Pixel: the number of pixels representing the tumor region in the ground truth mask; Tumor Pred: the number of tumor pixels predicted by the deep learning models; Correct Pixel: the number of correctly identified tumor pixels; Dice (%) – the Dice coefficient indicating the overlap between predicted and ground truth tumor regions; and Area is the estimated tumor area. DeepLabv3+ tends to overestimate tumor size, as seen in the first MRI image, where the actual tumor area is about 2,900 pixels, but the model predicts over 4,000 pixels. Such overestimation may trigger false alarms and affect clinical severity assessment.

FC-DenseNet exhibits a similar but less pronounced overestimation, suggesting a conservative coverage tendency that still requires fine-tuning to avoid excessive enlargement. ResU-Net delivers the most accurate area estimation, closely matching the ground truth while maintaining a high number of Correct Pixels, demonstrating both precision and stability. In contrast, U-Net often underestimates tumor size, significantly reducing the detected tumor pixel count, which risks missing small or peripheral lesions potentially critical in early diagnosis.

In medical applications, tumor area accuracy plays a critical role in assessing the extent of tumor invasion and supporting the development

of effective treatment plans. An effective model must not only correctly identify the tumor location but also accurately estimate its area. This ensures that physicians can avoid both overestimating the tumor size, which may cause unnecessary anxiety for the patient and hinder effective treatment, and underestimating it, which could lead to overlooking serious conditions. Table 2 presents a comparative analysis of tumor area estimations from the brain tumor segmentation results shown in Figure 9, obtained using different deep learning models: U-Net, ResU-Net, FC-DenseNet, and DeepLabv3+. Notably, tumor areas were calculated using Eq. (1).

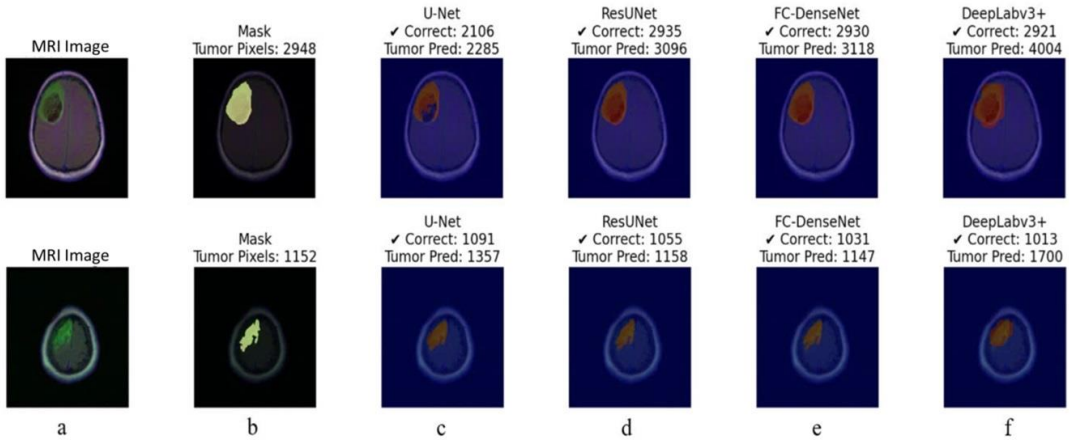

Figure 9. Tumor region estimation based on pixel count: (a) original MRI image; (b) ground truth mask; (c) predicted mask from U-Net; (d) predicted mask from ResU-Net; (e) predicted mask from FC-DenseNet; (f) predicted mask from DeepLabv3.

Table 2 presents a comparison of tumor area estimation performance among four deep learning models, U-Net, ResU-Net, FC-DenseNet, and DeepLabv3+, applied to two MRI cases (upper and lower panels of Figure 9). Overall, ResU-Net achieves the highest accuracy, yielding the smallest estimation errors of 11.27 mm² and 7.21 mm² for the upper and lower panels, respectively. This reflects its strong agreement with the ground truth and its ability to balance precise boundary detection with accurate size estimation, making it highly suitable for clinical applications. FC-DenseNet produces slightly higher errors (13.16 mm² and 8.12 mm²) but still maintains good accuracy, indicating that it can be a viable alternative with further fine-tuning. In contrast, U-Net shows a tendency to underestimate tumor areas, which, despite a relatively low error in the upper panel (12.53 mm²), risks missing tumor tissue, particularly in the lower panel. DeepLabv3+, on the other hand, consistently overestimates tumor sizes, producing the largest errors (75.81 mm² and 48.09 mm²) due to excessive segmentation, which could lead to false alarms and inappropriate treatment planning. These findings highlight that ResU-Net offers the most reliable tumor area estimation, with FC-DenseNet as a potential backup option, while U-Net and DeepLabv3+ require further adjustment to mitigate underestimation and overestimation issues, respectively.

3. CONCLUSION

This study implemented and evaluated the performance of the ResU-Net deep learning model for detecting and estimating the area of brain tumors from MRI images. To validate the effectiveness of the proposed approach, ResU-Net was compared with established models, including U-Net, FC-DenseNet, and DeepLabv3+. Experimental results demonstrate that ResU-Net not only achieves highly accurate tumor localization but also provides precise area estimation, outperforming the other models in both aspects. These promising results indicate that ResU-Net can significantly enhance brain tumor diagnosis by improving detection reliability and reducing human error in interpretation. With accurate tumor area estimation, clinicians can better assess disease severity across MRI scans, enabling more informed treatment planning and potentially improving patient outcomes.

Acknowledgments

REFERENCES

1 Appiah, R., Pulletikurthi, V., Esquivel-Puentes, H. A., Cabrera, C., Hasan, N. I., Dharmarathne,

S., Gomez, L. J. & Castillo, L. Brain tumor detection using proper orthogonal decomposition integrated with deep learning networks, *Computer Methods and Programs in Biomedicine*, **2024**, *250*, 108167.
2 Joshi, M. & Singh, B. K. Proportion estimation and multi-class classification of abnormal brain cells, *Medinformatics*, **2024**, *1*, 79-90.
3 Kumar, K., Jyoti, K. & Kumar, K. Machine learning for brain tumor classification: evaluating feature extraction and algorithm efficiency, *Discover Artificial Intelligence*, **2024**, *4*, 112.
4 Khalili, N., Shooli, H., Hosseini, N., Fathi Kazerooni, A., Familiar, A., Bagheri, S., Anderson, H., Bagley, S. J. & Nabavizadeh, A. Adding value to liquid biopsy for brain tumors: the role of imaging, *Cancers*, **2023**, *15*, 5198.
5 Loeber, S. MRI characteristics of primary brain tumors and advanced diagnostic imaging techniques, *Veterinary Clinics: Small Animal Practice*, **2025**, *55*, 23-39.
6 Sabeghi, P., Zarand, P., Zargham, S., Golestany, B., Shariat, A., Chang, M., Yang, E., Rajagopalan, P., Phung, D. C. & Gholamrezanezhad, A. Advances in Neuro-Oncological imaging: an update on Diagnostic Approach to Brain tumors, *Cancers*, **2024**, *16*, 576.
7 Rubinger, L., Gazendam, A., Ekhtiari, S. & Bhandari, M. Machine learning and artificial intelligence in research and healthcare, *Injury*, **2023**, *54*, S69-S73.
8 Tilala, M. H., Chenchala, P. K., Choppadandi, A., Kaur, J., Naguri, S., Saoji, R., Devaguptapu, B. & Tilala, M. Ethical considerations in the use of artificial intelligence and machine learning in health care: a comprehensive review, *Cureus*, **2024**, *16*, 62443.
9 Bala, S. A. & Kant, S. Dense dilated inception network for medical image segmentation, *international Journal of Advanced Computer Science and Applications*, **2020**, *11*, 785-793.
10 Gite, S., Mishra, A. & Kotecha, K. Enhanced lung image segmentation using deep learning, *Neural Computing and Applications*, **2023**, *35*, 22839-22853.
11 Zhang, Z., Wu, C., Coleman, S. & Kerr, D. DENSE-INception U-net for medical image segmentation, *Computer methods and programs in biomedicine*, **2020**, *192*, 105395.
12 Anaya-Isaza, A., Mera-Jiménez, L. & Zequera-Diaz, M. An overview of deep learning in medical imaging, *Informatics in medicine unlocked*, **2021**, *26*, 100723.
13 Gómez-Guzmán, M. A., Jiménez-Beristaín, L., García-Guerrero, E. E., López-Bonilla, O. R., Tamayo-Perez, U. J., Esqueda-Elizondo, J. J., Palomino-Vizcaino, K. & Inzunza-González, E. Classifying brain tumors on magnetic resonance imaging by using convolutional neural networks, *Electronics*, **2023**, *12*, 955.
14 Musallam, A. S., Sherif, A. S. & Hussein, M. K. A new convolutional neural network architecture for automatic detection of brain tumors in magnetic resonance imaging images, *IEEE access*, **2022**, *10*, 2775-2782.
15 Azad, R., Aghdam, E. K., Rauland, A., Jia, Y., Avval, A. H., Bozorgpour, A., Karimijafarbigloo, S., Cohen, J. P., Adeli, E. & Merhof, D. Medical image segmentation review: The success of u-net, *IEEE Transactions on Pattern Analysis and Machine Intelligence*, **2024**, *46*, 10076-10095.
16 Sabir, M. W., Khan, Z., Saad, N. M., Khan, D. M., Al-Khasawneh, M. A., Perveen, K., Qayyum, A. & Azhar Ali, S. S. Segmentation of liver tumor in CT scan using ResU-Net, *Applied Sciences*, **2022**, *12*, 8650.
17 Wang, Z., Li, X., Yao, M., Li, J., Jiang, Q. & Yan, B. A new detection model of microaneurysms based on improved FC-DenseNet, *Scientific Reports*, **2022**, *12*, 950.
18 Prokopiou, I. & Spyridonos, P. Highlighting the Advanced Capabilities and the Computational Efficiency of DeepLabV3+ in Medical Image Segmentation: An Ablation Study, *BioMedInformatics*, **2025**, *5*, 10.
19 Aljohani, A. & Alharbe, N. Enhancing Medical Image Segmentation through Stacked U-Net Architectures with Interconnected Convolution Layers, *Egyptian Informatics Journal*, **2023**, *31*, 100753.
20 Assam, M., Kanwal, H., Farooq, U., Shah, S. K., Mehmood, A. & Choi, G. S. An efficient classification of MRI brain images, *IEEE Access*, **2021**, *9*, 33313-33322.
21 Kamiri, J., Wambugu, G. M. & Oirere, A. M. An Empirical Analysis of Encoder Decoder (U Net) Variants for Medical Image Segmentation, *International Journal of Scientific Research in Computer Science and Engineering*, **2025**, *13*, 26-31.
22 Luo, Y., Xu, L. & Qi, L. A cascaded FC-DenseNet and level set method (FCDL) for fully automatic segmentation of the right ventricle in cardiac MRI, *Medical & Biological Engineering & Computing*, **2021**, *59*, 561-574.
23 Fadhl, A. A. M., Al-rimy, B. A. S., Almalki, S. A., Alghamdi, T., Alkhorem, A. H. & Sheldon, F. T. Enhancing steganography security with generative AI: a robust approach using content-adaptive techniques and FC DenseNet, *International Journal of Advanced Computer Science and Applications*, **2024**, *15*, 933-941.
24 Saleem, N., Gunawan, T. S., Shafi, M., Bourouis, S. & Trigui, A. Multi-attention bottleneck for gated convolutional encoder-decoder-based speech enhancement, *IEEE Access*, **2023**, *11*, 114172-114186.
25 Song, J., Zheng, Y., Wang, J., Ullah, M. Z., Li, X., Zou, Z. & Ding, G. Multi-feature deep information bottleneck network for breast cancer classification in contrast enhanced

spectral mammography, *Pattern Recognition*, **2022**, *131*, 108858.

26 Peng, H., Xue, C., Shao, Y., Chen, K., Xiong, J., Xie, Z. & Zhang, L. Semantic segmentation of litchi branches using DeepLabV3+ model, *Ieee Access*, **2020**, *8*, 164546-164555.

27 Ataş, İ. Performance evaluation of jaccard-dice coefficient on building segmentation from high resolution satellite images, *Balkan Journal of Electrical and Computer Engineering*, **2023**, *11*, 100-106.

28 Vlăsceanu, G. V., Tarbă, N., Voncilă, M. L. & Boiangiu, C. A. Selecting the right metric: A detailed study on image segmentation evaluation, *BRAIN. Broad Research in Artificial Intelligence and Neuroscience*, **2024**, *15*, 295-318.